Dependence of acetate based anti-solvent for high humidity fabrication of $CH_3NH_3PbI_3$ perovskite devices in ambient atmosphere

*Fu Yang, Gaurav Kapil, PuTao Zhang, Zhaosheng Hu, Muhammad Akmal Kamarudin, Tingli Ma, Shuzi Hayase**

Kyushu Institute of Technology, 204 Hibikino Wakamatsu-ku, Kitakyushu 808-0196, Japan

ABSTRACT

High efficiency perovskite solar cells (PSCs) need to be fabricated in the nitrogen filled glove box by atmosphere-controlled crystallization process. However, the use of glove box process is of great concern for mass level production of PSCs. In this work, notable efficient $CH_3NH_3PbI_3$ solar cells can be obtained in high humidity ambient atmosphere (60%-70% relative humidity) by using acetate as anti-solvent, in which dependence of methyl, ethyl, propyl, and butyl acetate on the crystal growth mechanism are discussed. It is explored that acetate screens the sensitive perovskite intermediate phases from water molecules during perovskite film formation and annealing. It is revealed that relatively high vapor pressure and high water solubility of methyl acetate (MA) leads to the formation of highly dense and pinhole free perovskite films guiding to the best power conversion efficiency of 16.3% with a reduced hysteresis. The devices prepared using MA showed

remarkable shelf life stability of more than 80% for 360 hours in ambient air condition, when compared to the devices fabricated using other anti-solvents with low vapor pressure and low water solubility. Moreover, the PCE still kept at 15.6% even though 2 v% deionized water was added in the MA for preparing the perovskite layer.

INTRODUCTION

Organometallic halide perovskite solar cells (PSCs) have attracted considerable attention around the world owing to the high absorption coefficient, ambipolar charge transport, long diffusion length, and fast mobility of both electrons and holes.[1-6] The efficiency of solid-state PSCs has increased from 3.8 % in 2009 to 22.7 % so far, which is much higher than other third-generation solar cells.[7-8] Besides their remarkable photovoltaic performance, the easy and cheap solution-based fabrication process also could lower the fabrication cost and promote their wide commercialization around the world.[9-11] One of key points for preparing high-performance PSCs is to control the morphology and crystal structure of perovskite materials. Numerous techniques for preparing the perovskite films have been reported, such as one-step spin-coating, sequential deposition, thermal evaporation and vapor processing of components.[12-15] One-step spin-coating method is widely used for fabricating the perovskite layer, as the method is simple to control. However, the films always have incomplete surface coverage and poor morphology, which results in charge recombination in solar cells. To address this issue, anti-solvent washing method has been developed using solvents such as chlorobenzene, toluene, or diethyl ether during spin-coating process of perovskite films. A mixture of N,N-dimethylformamide (DMF) and dimethyl sulfoxide (DMSO) is well known polar solvents for the preparation of perovskite precursor solution. The function of the anti-solvent is to remove the high boiling point solvent DMF and form a transparent

intermediate adduct (CH_3NH_3I-PbI_2-DMSO) from its perovskite precursor solution, which leads to a smooth, pinhole free and homogenous perovskite film with high electronic properties.[16]

Despite the high efficiency of PSCs, the perovskite layer is very sensitive to moisture and easily degrades in high humidity either during fabrication process or device measurement.[17-19] To solve this problem, most researchers prepared PSCs inside nitrogen/argon filled glovebox to avoid water, which increases the solar cells manufacturing cost. Therefore, research in the area of fabricating perovskite films in ambient air is desirable. Yan and co-workers reported use of lead (II) thiocyanate ($Pb(SCN)_2$) precursor for fabricating $CH_3NH_3PbI_{3-x}(SCN)_x$ PSCs in more than 70 % humidity showing efficiency up to 15 %.[20] With the assistance of hydrochloric acid, Zhao and co-workers prepared high-quality $CH_3NH_3PbI_3$ perovskite films in ~60 % humidity.[21] Recently, Watson and co-workers used ethyl acetate as an anti-solvent during one-step deposition; where they suggested that ethyl acetate acted as a moisture absorber protecting sensitive perovskite intermediate phases from water molecules during film formation and annealing.[22] However, there are still quite few reports on one-step deposition of perovskite film in the high humidity ambient air condition.

In this report, four different acetate-based solvents (methyl acetate (MA), ethyl acetate (EA), propyl acetate (PA), butyl acetate (BA)) were used as the anti-solvent for preparing high-quality $CH_3NH_3PbI_3$ perovskite film in high humidity (60-70 % RH) air condition. It was explored that MA could give a high-quality perovskite film with more homogeneous morphology than other three kinds of acetate anti-solvents. Upon optimization, the best solar cell by MA washing exhibited a stabilized PCE of 16.3% with low hysteresis. Moreover, the PCE still kept at 15.6 % even though 2 v% deionized water was added in the MA for preparing the perovskite layer. We

believe that this study would give a good direction for PSCs fabrication in humid climate and uncontrolled laboratories, potentially enabling the commercialization of devices.

RESULTS AND DISCUSSION

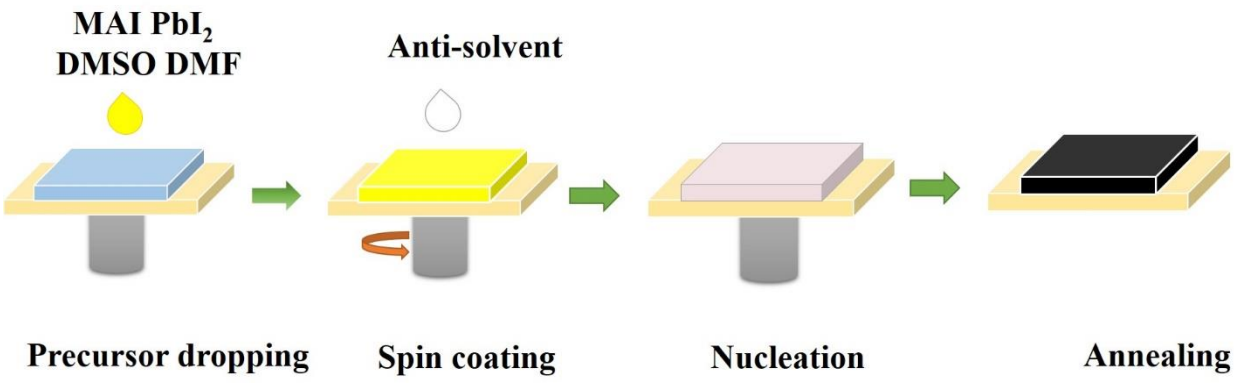

Figure 1. Schematic illustration of the one-step process using anti-solvent for fabricating perovskite films.

In the anti-solvent based one-step preparation process, the perovskite layer is formed by spin coating of the precursor solution followed by the thermal annealing. This preparation process usually has two stages, which shown in Figure 1. In the first stage, the liquid film is thinning by the centrifugal forces. After a transition point, evaporation rate of the solvent dominates the film thinning, which depends on the vapor pressure of the solvent. Then at the second stage, solution becomes supersaturated, nucleation happens and growths, solid intermediate (or perovskite) film forms. Thus, in order to prepare high-quality perovskite film, the important stage is to accelerate the evaporation rate of excess DMF and control the perovskite crystallization process.[23] For two immiscible solvents, the total vapor pressure of the mixed solution is close to the plus of the two solvents' vapor pressures, and the boiling point of the mixture should be lower than each solvent.[24] Follow this rule, introducing the high vapor pressure anti-solvent for one-step preparing perovskite film will help promote a uniform and high-quality film.

As perovskite layer is sensitive to moisture within the air during spin coating. Watson and co-workers proposed that when using EA as the anti-solvent in one-step deposition, moisture in the air is preferred in solution with the anti-solvent rather than reacting with the perovskite intermediate phase.[22] So one way to solve this problem is to introduce more water-soluble anti-solvent to avoid the water absorption of the perovskite intermediate phase during the spin coating process. In addition, after the perovskite intermediate phase formed, it is better to reduce contacting time of this intermediate phase with the moisture within the air to avoid the water affection. Therefore, the second way is to speed up the perovskite forming procession to reduce the formation time of perovskite intermediate phase to perovskite. So from the above discussions, we assume that using the solvent which has high vapor pressure and more water solubility as the anti-solvent in one step spin-coating progression will be great helpful to fabricate a high-quality perovskite film.

Table 1. Physical properties (vapor pressure, boiling point, solubility in water) of solvents.

Solvent	Vapor pressure at 25 ^{o}C (Kpa)	Boiling point (^{o}C)	Solubility in H_2O (g/100 mL)
MA	28.8	56.9	24.4
EA	12.4	77.1	8
PA	4.8	101.5	1.6
BA	1.1	126.1	0.68

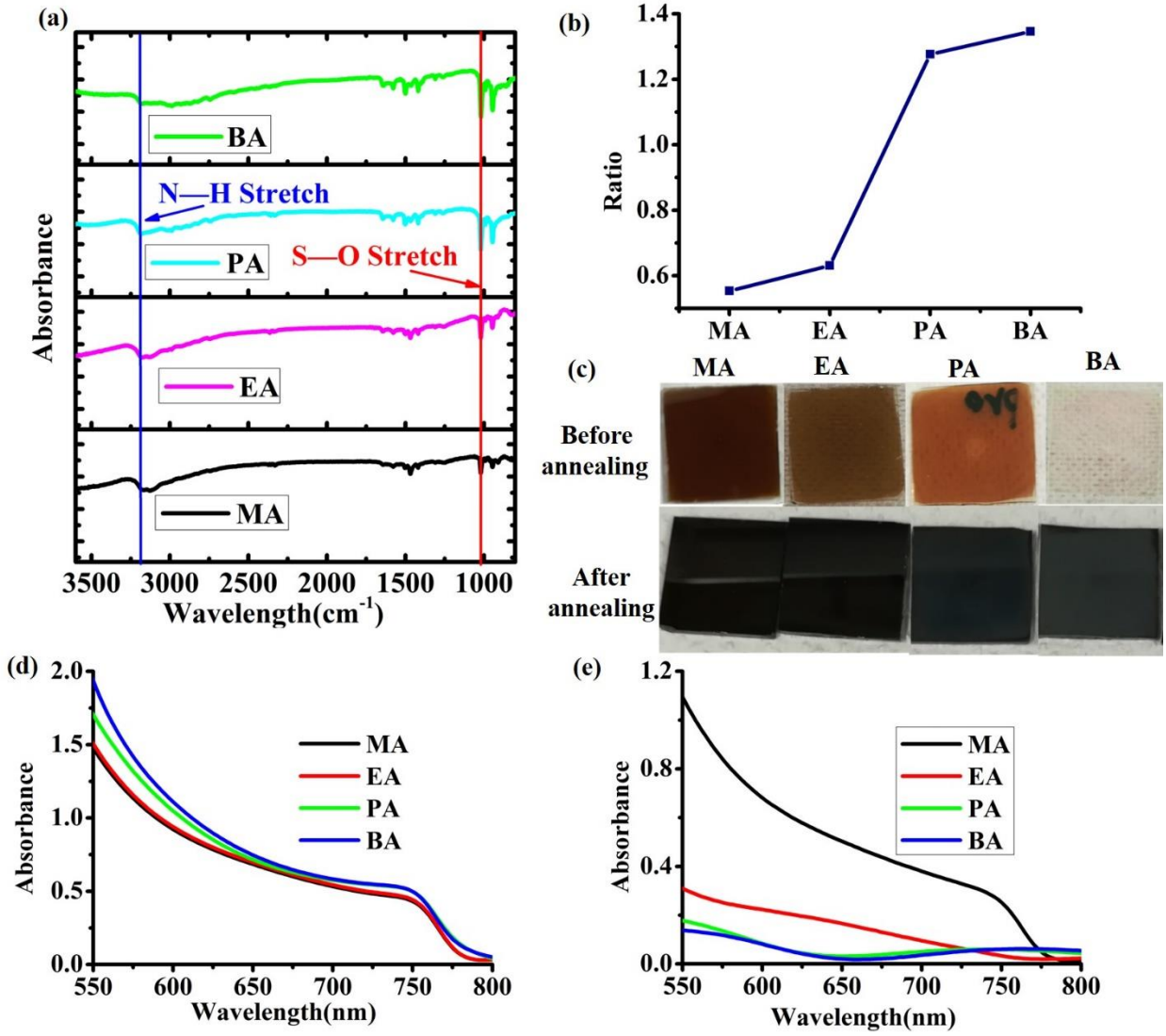

Figure 2. (a) Attenuated Total Reflectance Fourier transform IR spectra of $CH_3NH_3PbI_3$ films (on Pt/glass substrates) prepared by MA, EA, PA and BA without annealing. (b) Ratio of intensity of absorbance at 1050 cm^{-1} and 3190 cm^{-1} (1050 cm^{-1} : 3190 cm^{-1}). (c) The perovskite film on FTO/compact SnO_2 after spinning by different anti-solvents before and after annealing. (d) UV-vis absorption spectra of perovskite films prepared with by different solvents without annealing and (e) with annealing.

Physical properties (vapor pressure, boiling point and water solubility) of the four acetate-based solvents were illustrated in Table 1. Among those four acetates, MA had the relative highest vapor pressure (28.8 Kpa), lowest boiling point (56.9 ºC) and best water solubility. The high vapor pressure and low boiling point would accelerate the evaporation rate of excess DMF and control the perovskite crystallization process. Moreover, the more water solubility of the anti-solvent could decrease the moisture affection of the perovskite intermediate phase during the spin coating process. Hence, it could be noticed that perovskite fabrication by MA treatment would give a high-quality perovskite film with more homogeneously morphology than other three acetates (EA, PA, BA).

Figure 2a showed FT-IR spectra of $CH_3NH_3PbI_3$ film prepared with different anti-solvents (MA, EA, PA and BA) without annealing. The non-annealing films showed similar absorbance peak positions. All the films showed N-H vibration peaks at 3200 cm^{-1} and at approximately 1470 cm^{-1} attributed to CH_3NH_3I, and S-O stretching at 1020 cm^{-1} attributed to DMSO.[25] By taking the ratio (absorbance at 1020 cm^{-1} to the absorbance at 3200 cm^{-1}), the concentration of DMSO in the intermediate phase can be deduced. From this ratio, it was found that the DMSO content decreased form MA to BA, as shown in the Figure 2b. The less DMSO ratio mean the few intermediate phase of CH_3NH_3I-PbI_2-$DMSO_x$, which indicated the speeding up of perovskite formation process.[26] Figure 2c showed the fresh perovskite film by different anti-solvents with or without annealing. The color of the annealing-free film gradually changed from dark brown (MA) to transparent (BA), which meant increased DMSO content in the intermediate phase films.[27] This result was in agreement with the FT-IR spectra. Furthermore, the annealed films exhibited decreased glossiness of the perovskite films from MA to BA, which indicated that the $CH_3NH_3PbI_3$ perovskite films became more inhomogeneous. Ahn et al. reported that the DMSO intermediate phase was

unfavorable due to the gradual vaporization of DMSO from the surface of the spin-coated film, which led to an inhomogeneous $CH_3NH_3PbI_3$ film.[16] Figure 2d and 2e showed the absorption spectra of perovskite films prepared by different anti-solvents treatment before and after annealing. The UV-vis absorption spectrum of a freshly perovskite film prepared by MA treatment was almost close to that of the annealed film, indicating that the using of MA resulted in nearly complete $CH_3NH_3PbI_3$ crystallization at room temperature. Therefore, from the above results, we concluded that a large amount of redundant DMSO in the annealing-free perovskite layers might be harmful for the performance of PSCs when preparing perovskite in high humidity air condition.

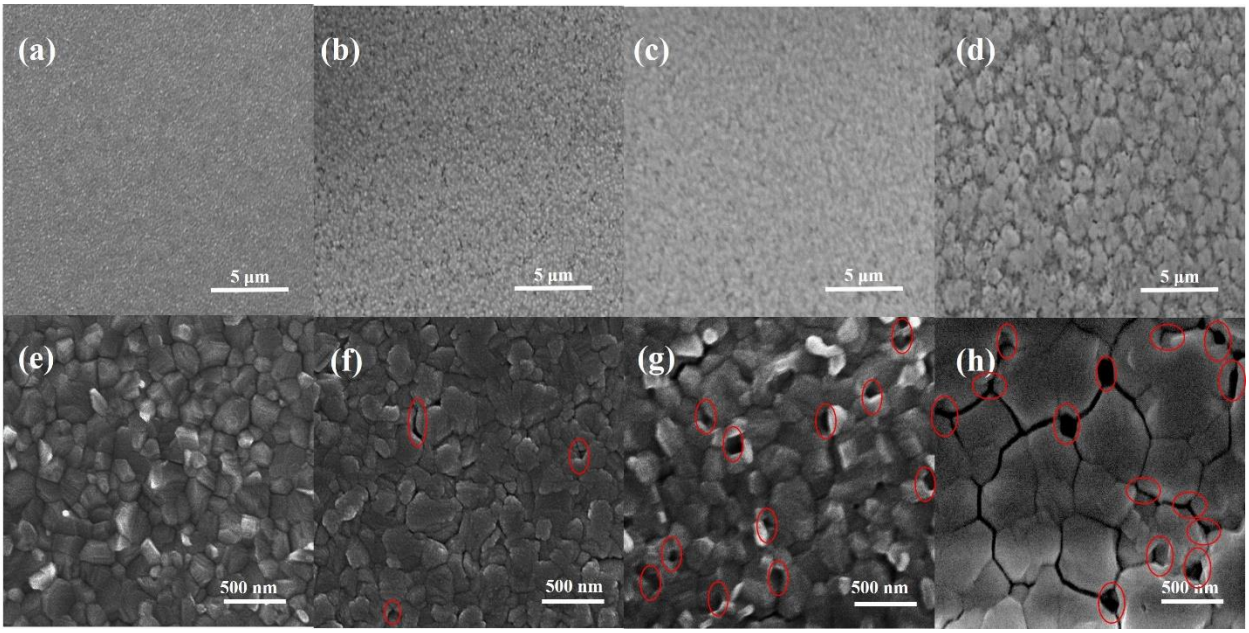

Figure 3. The scanning electron microscopy of annealed $CH_3NH_3PbI_3$ films of FTO/Compact SnO_2 by different anti-solvents. (a), (e) MA; (b) (f) EA; (c) (g) PA; (d) (h) BA.

Figure 3 showed the surface morphology of the annealed $CH_3NH_3PbI_3$ perovskite films based on different anti-solvents by scanning electron microscopy (SEM). The perovskite film prepared by MA treatment showed extremely dense, homogeneous and almost no pinholes, which shown in Figure 3a and 3e. However, with EA treatment, the perovskite film became slightly

inhomogeneous and the presence of pinholes could be observed in Figure 3b and 3f. Especially in the case of BA, the presence of pinholes was very prominent (Figure 3d and 3h). This result was consistent with the image in Figure 2c where the film appeared the least luminous. Moreover, the grain size of the $CH_3NH_3PbI_3$ perovskite gradually increased, which maybe owning to the increase of DMSO content in the intermediate perovskite phase.[11]

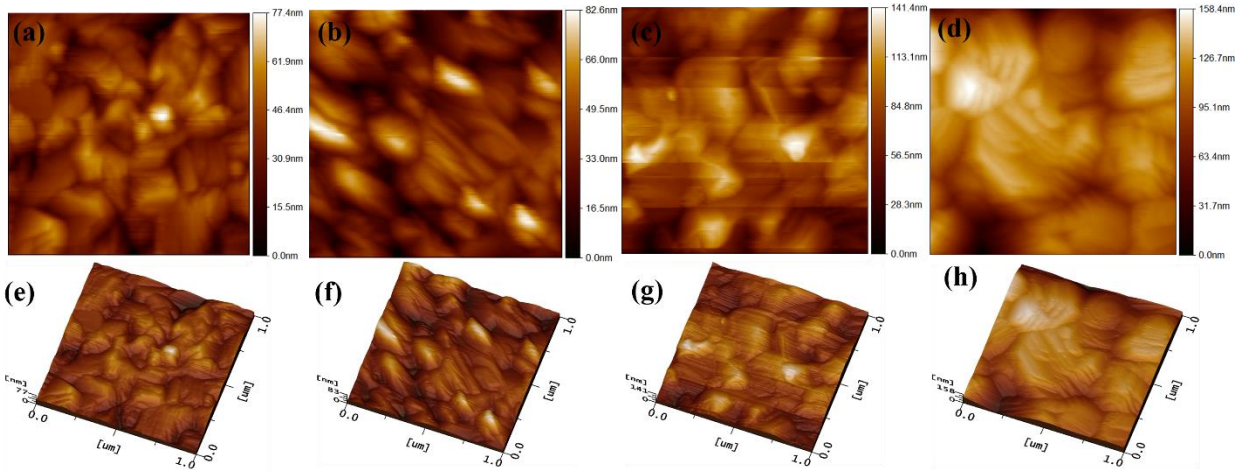

Figure 4. Atomic force microscopy (AFM) height (a, b, c, d) and 3D surface plot images (e, f, g, h) of the perovskites film on FTO/SnO_2 prepared by MA (a, e) or EA (b, f), PA (c, g) and BA (d, h) treatment processes. The scanning range of the images is 1 μm×1 μm.

Atomic force microscopy (AFM) was employed to study the surface morphology perovskite films prepared by different anti-solvents, as shown in Figure 4. The annealing time was fixed at 10 min. It was found that the grain sizes of perovskite samples were graduate increased by the treatment way from MA, EA, PA, to BA, which was in consistence with Figure 3. The Rq roughness values were measured to be 10.2, 13.8, 22.7 and 25.8 nm for samples prepared by MA, EA, PA and BA, respectively. The roughness value was smallest for perovskite film prepared by MA treatment, and increased from MA, EA, PA to BA, which is in accordance with the Figure 3a-d. The 3D surface

plot images shown in Figure 4e-h could clearly show the increase of the surface roughness for perovskite films. This surface topography indicated that perovskite films prepared by MA had better coverage on the top of perovskite film, resulting in larger parallel resistance and lower serial resistance, as evidenced by the improved diode characteristics.

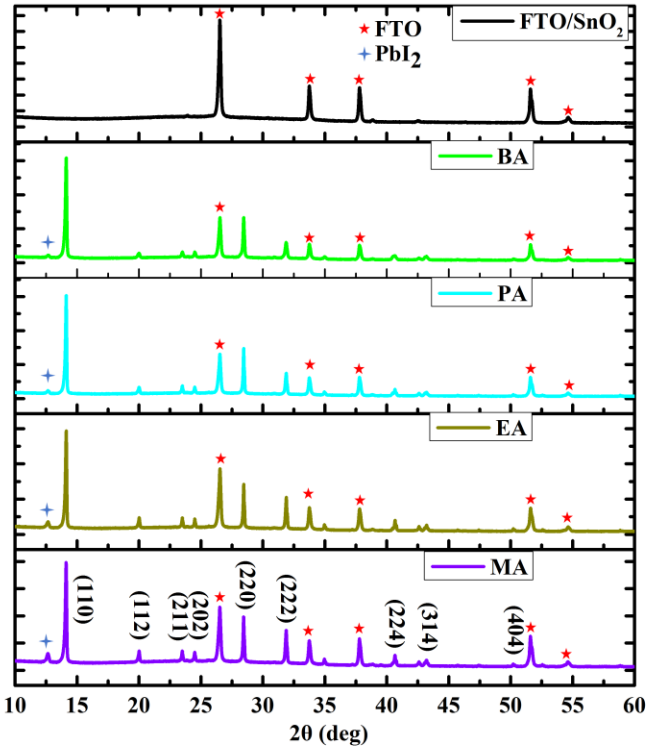

Figure 5. X-ray diffraction (XRD) of $CH_3NH_3PbI_3$ films on FTO/compact SnO_2 substrates prepared by different anti-solvents.

Figure 5 showed the X-ray diffraction (XRD) patterns of $CH_3NH_3PbI_3$ layer on FTO/SnO_2 substrate with different anti-solvents. Peaks from the substrates were indicated by triangles. Strong diffraction peaks located at 14.1°, 20.0°, 23.5°, 24.5°, 28.4°, 31.9°, 40.7°, 43.1° and 50.2° for 2θ scan were observed corresponding to the planes of (110), (112), (211), (202), (220), (222), (224), (314) and (404), which were in good agreement with the previous reports.[15, 28-29] The result confirmed the films are highly crystallized perovskite phase.[30-31] Meanwhile, a weak diffraction

pattern of PbI_2 appeared at 12.7°, where the intensity of the peak decreases upon changing the anti-solvent from MA to BA. This decrease of PbI_2 content in perovskite film could be ascribed to the different solubility of PbI_2 and CH_3NH_3I compounds in various anti-solvents.[32] Although there were many discussions about the function of residual PbI_2, it was hard to tell the exact impact of such little remaining PbI_2 on this anti-solvent process for perovskite formation.

Table 2. Devices performance data of FTO/c-SnO_2/$CH_3NH_3PbI_3$/Spiro-OMeTAD/Au by different anti-solvents.

Solvent	Classification	V_{oc} (V)	J_{sc} (mA/cm^2)	FF (%)	PCE (%)
MA	Champion [a]	1.05	22.21	70.0	16.3
	Average [b]	1.04±0.02	21.78±0.45	68.9±1.42	15.6±0.7
EA	Champion	1.04	21.71	66.9	15.1
	Average	1.02±0.03	21.44±0.82	64.6±3.89	14.2±1.1
PA	Champion	0.97	20.67	66.8	13.4
	Average	0.95±0.05	20.30±0.75	62.9±5.60	12.2±1.0
BA	Champion	0.96	19.97	66.5	12.7
	Average	0.94±0.04	20.26±0.34	60.4±2.61	11.4±0.7

a, the best performance of PSCs. b, the average performance of 20 PSCs.

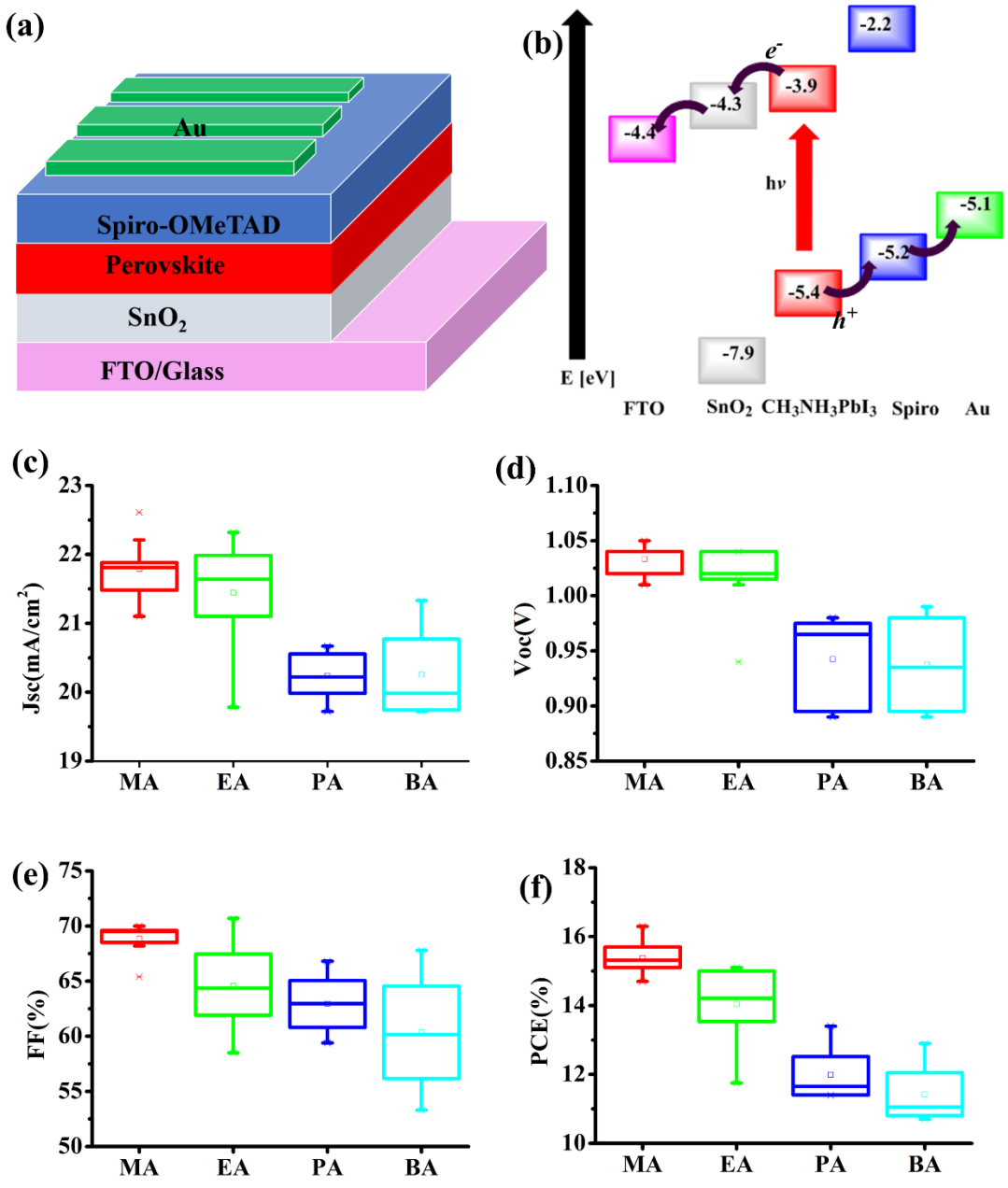

Figure 6. Schematic structure (a) and (b) energy diagram of the planar FTO/c-SnO2/ $CH_3NH_3PbI_3$/Spiro-OMeTAD/Au planar perovskite solar cells. Photovoltaic statistics for the planar perovskite solar cells processed by anti-solvents. (c) Short-circuit current, (d) Open circuit voltage, (e) Fill factor, (f) Efficiency. The boxes represent 80 data from the V_{oc}-to-J_{sc} scan direction.

To show the reproducibility of devices efficiency, the PCEs of 20 planar perovskite solar cells prepared by different anti-solvents were measured. High efficiency PSCs generally uses titanium oxide (TiO_2) as an electron transport layer; however, some drawbacks such as UV light instability because of the photocatalytic activity hinder reproducibility over the time. Tin-oxide (SnO_2) as an alternative to TiO_2, has been reported to exhibit better electron mobility and stability. In addition, a higher band gap with deep valence band maximum is supposed to effectively block the photo-generated holes from the absorber layer to recombine with the electrons in conducting oxide layer (TCO). Therefore, a planar PSC structure employing SnO_2 was chosen for preparing high-quality $CH_3NH_3PbI_3$ perovskite films in high humidity (60-70% RH). Figure 6a and 6b exhibited schematic structure and energy diagram of the PSCs. The current density-voltage (J-V) performance data were shown in Figure 6c-f, and Table 2 summarized the photovoltaic parameters of the solar cells. There was a clear decreasing trend of all the parameters of PSCs (V_{oc}, J_{sc}, FF, PCE) among the four anti-solvents treatments, because of the inhomogeneous perovskite layer.[33-35] We could see from Figure 6c-f that an average V_{oc} of 1.04±0.02 V, J_{sc} of 21.78±0.45 mA/cm^2, FF of 68.9±1.42 %, and PCE of 15.6±0.7 % were obtained for devices fabricated using MA treatment. The champion device of MA treatment perovskite devices had a V_{oc} of 1.05 V, a J_{sc} of 22.21 mA/cm^2, a FF of 70.0 % and an efficiency of 16.3 %. Such high efficiency could be attributed to the reproducible and uniform growth of $CH_3NH_3PbI_3$ layer obtained by anti-solvent deposition process. The performance of EA treated perovskite film was marginally lower than MA with an average V_{oc} of 1.02±0.03 V, J_{sc} of 21.44±0.82 mA/cm^2, FF of 64.6±3.89 %, and PCE of 14.2±1.1 %. However, the performances with PA and BA treatments decreased significantly, with an average V_{oc} of 0.95±0.05 V, J_{sc} of 20.30±0.75 mA/cm^2, FF of 62.9±5.60 %, PCE of 12.2±1.0 %, and V_{oc} of 0.94±0.04 V, J_{sc} of 20.26±0.34 mA/cm^2, FF of 60.4±2.61 %, PCE of 11.4±0.7 %,

respectively. Figure 7 showed the J-V curves and the corresponding IPCE for the PSCs. The calculated J_{sc} from the IPCE agreed well with the measured J_{sc}. Figure S3 demonstrated the J-V curve of reverse direction and forward direction. Importantly, intended to quantitatively compare the hysteresis effect across diverse samples, a modified hysteresis index (HI) values were calculated from the J-V curves, shown in Figure 7a.[36] The hysteresis of the solar cell performance indicated an approximate increasing trend, which was demonstrated by the HI values of MA (HI, 0.10), EA (0.21), PA (0.40) and PA (0.56).

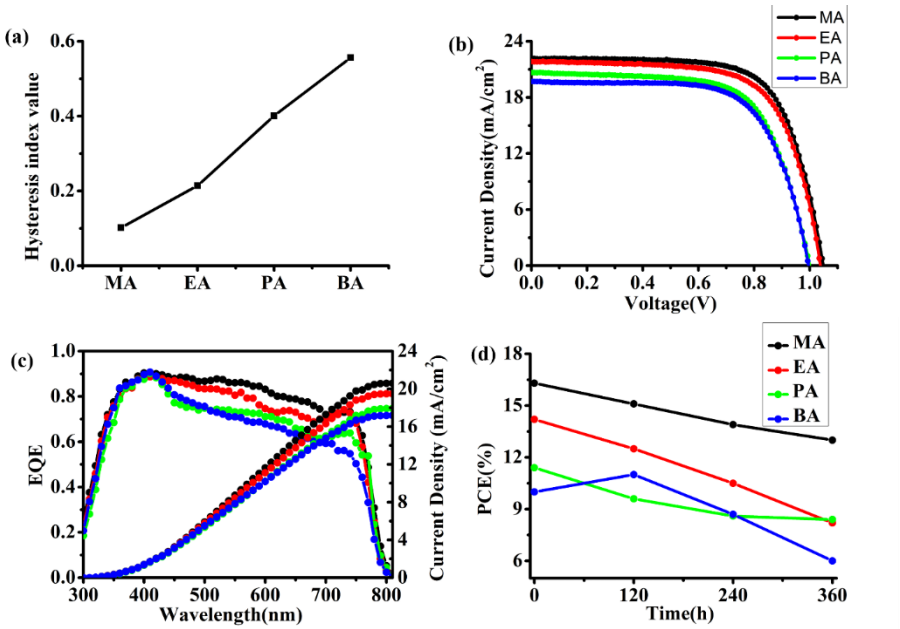

Figure 7. (a) Hysteresis index value calculated from the J-V curve of four acetate based champion devices. J-V (b) and the correspondent IPCE (c) curves of different anti-solvents based planar FTO/c-SnO_2/$CH_3NH_3PbI_3$/Spiro-OMeTAD/Au champion devices. (d) Stability test for 360 h of the different anti-solvents based planar FTO/c-SnO_2/$MAPbI_3$/Spiro-OMeTAD/Au devices under ambient atmosphere without sealing, and the average humidity is about 60% RH.

Furthermore, the indoor environment stability of the different anti-solvents processed devices were investigated as shown in Figure 7a. The perovskite devices were stored at ambient room temperature and under controlled humidity about 60-70% RH without sealing. After 360 h, the PCE of the perovskite devices prepared by MA treatment still retain over 80% of its original efficiency, while the PCE of perovskite devices prepared by the other three acetates decreased to less than 60% of the fresh devices. It is interesting to note that all the PSC devices` fabrication processes were accomplished in the 60-70% RH air condition. In addition, for comparison, the devices based on commonly used anti-solvents (diethyl ether, chlorobenzene, and toluene) were also prepared in the 60-70% RH air condition. However, all those devices showed poor performances compared to acetate-based solvents (Table S1). Hence, it is safe to assume that the MA treated devices are the most stable compared with other acetate solvents processed devices.

Watson and co-workers claimed that when using EA as the anti-solvent in one-step deposition perovskite film, the moisture in air tend to mix with the anti-solvent rather than with the perovskite intermediate phase.[22] Therefore, we assumed high water solubility of the anti-solvent would be beneficial during the fabrication of PSCs. In order to prove this hypothesis, 2 v % deionized water was deliberately added to the anhydrous MA, EA, PA and BA were used during the fabrication of PSCs. The current density-voltage (J-V) performance data were shown in Figure 8, and the resulting photovoltaic parameters of the solar cells were summarized in Table S2. In the case of MA, the addition of 2 v % deionized water had nearly no influence on devices performance with high efficiency of 15.6 % (average PCE, 14.8±0.5 %, kept at 94%). However, for the other three acetates, there was a significant decrease in the device performance from EA (average PCE, 9.9±1.7 %, kept at 69.5 %), PA (average PCE, 5.1±1.2 %, kept at 42.5 %) to BA (average PCE,

2.9±1.1 %, kept at 25.4 %). This could be attributed to the high solubility of water in MA which screens the perovskite film from getting dissipated by water molecules.

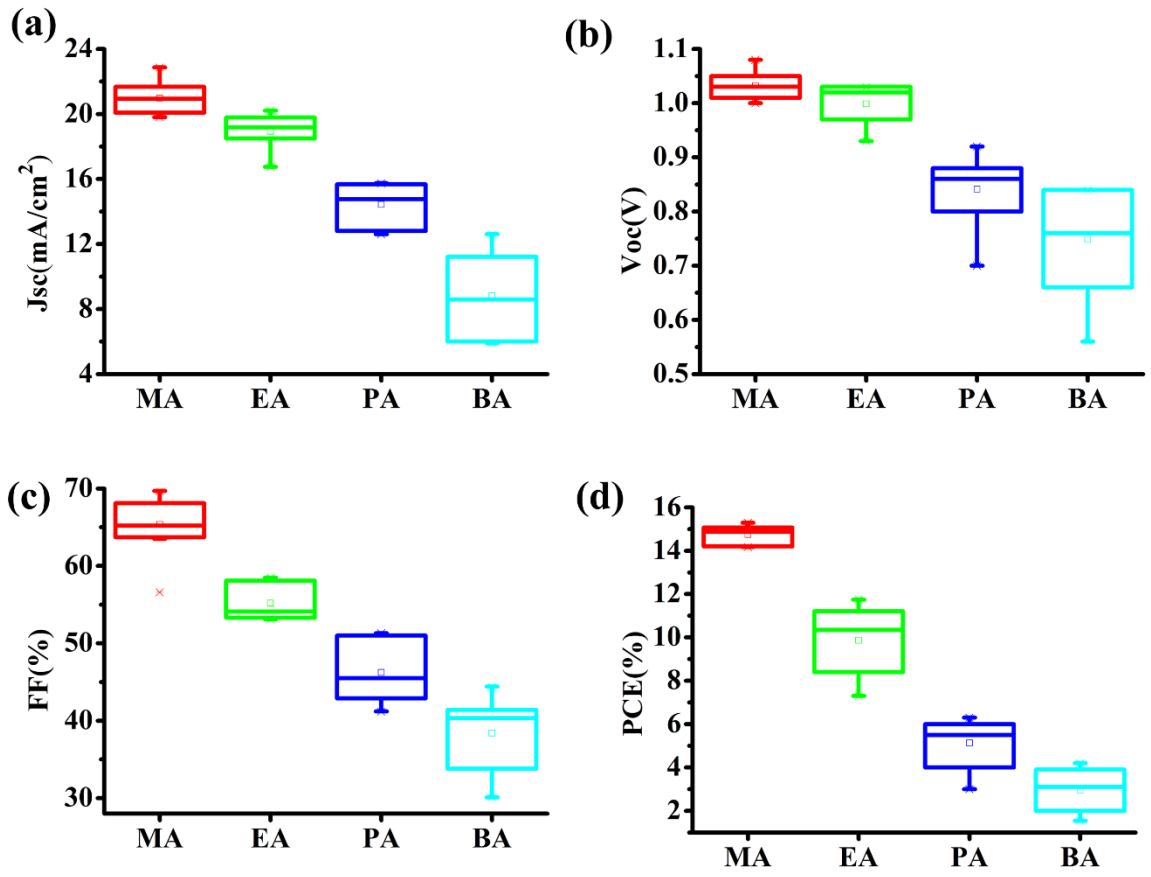

Figure 8. Photovoltaic statistics for FTO/c-SnO_2/$CH_3NH_3PbI_3$/Spiro-OMeTAD/Au planar perovskite solar cells processed by 2 v% deionized water added into anti-solvents. (a) Short-circuit current, (b) Open circuit voltage, (c) Fill factor, (d) Efficiency. The boxes represent 40 data from the V_{oc}-to-J_{sc} scan direction.

CONCLUSION

In conclusion, four different acetate-based solvents (MA, EA, PA, BA) were used as anti-solvent for preparing the $CH_3NH_3PbI_3$ PSCs in high humidity ambient atmosphere (60%-70% RH). The

highest solar cell efficiency was obtained with $CH_3NH_3PbI_3$ perovskite layer prepared by employing MA, showing the best PCE of 16.3% along with the improved photovoltaic parameters such as V_{oc} of 1.05 V, J_{sc} of 22.21 mA/cm^2, FF of 70.0%. Moreover, the performance decreases from using MA to BA. In addition, the stability test was performed which showed the superior performance of the MA based perovskite solar cell, reserving more than 80% of its original performance. The notable performance of the solar cell was attributed to the better film morphology of the perovskite film with condensed grains and no pinholes. The high water solubility of MA also meant that the perovskite layer was protected from contact with water due to the water molecules tend to remain in MA as the PCE still kept at 15.6 % when 2 v% deionized water added in MA for preparing PSCs. All the experiments were accomplished without the requirement for stringent atmospheric control. This study would give a direction for PSC production at commercial level in robust environment, which could lower the cost and reduce the time for fabricating the high efficiency PSCs.

EXPERIMENTAL SECTION

Preparation of perovskite solar cells.

All reagents were directly used without further purification, if not specified. F-doped SnO_2 layered glass (FTO glass, Nippon Sheet Glass Co. Ltd) glass was first patterned and cleaned by using Zinc powder and 6 N hydrochloric acid solution. Tin (II) chloride (Aldrich, 98%) was dissolved in anhydrous ethanol (Wako, 99.8%) to form a 0.1 M $SnCl_2$ concentration solution. Then the $SnCl_2$ solution was spun on the FTO glass at 2000 rpm for 30 seconds. The substrate was heated at 100 °C for 5 minutes and then annealed at 180 °C for 60 minutes on a hot plate to get a compact SnO_2 electron transport layer.[37] 1.5 M $CH_3NH_3PbI_3$ in anhydrous dimethylformamide (DMF, Aldrich,

99.8%) and anhydrous dimethyl sulfoxide (DMSO, Aldrich, 99.8) solution (DMF: DMSO, 4:1) were prepared by mixing equal molar ratio of CH_3NH_3I (TCI, 98%) and PbI_2 (TCI, 99.99%) and stirred at room temperature for more than 1 hour. The perovskite precursor solution was spun on the substrate at 4000 rpm for 25 seconds and 10 seconds after starting the spin-coating process, 0.5 mL of the anti-solvent was slowly dropped onto the film. After that, the immediate perovskite phase was heated at 65 °C for 1 minute and 100 °C for 10 minutes. The spiro-MeOTAD layer was prepared by spin coating a chlorobenzene solution containing 180 mM spiro-MeOTAD (Aldrich, 99 %), 60 mM tert-butylpyridine (Aldrich, 96 %), 30 mM Li-TFSI (Aldrich, 99.95 %) (520 mg/mL in acetonitrile) and 33 mM FK209 (Aldrich, 99 %) (300 mg/mL in acetonitrile) at 4000 rpm for 30 seconds. Finally, a 80 nm thickness Au counter electrode was deposited by thermal evaporation. All procedures were performed in 60-70 % relative humidity ambient air condition, Relative humidity was recorded using a hygrometer accurate to ± 5% RH between 25 % and 69.9 % RH, ±10 % RH between 70 % and 90.0 % RH) (A&D Company, AD-5681).

Characterization

Solar cell performances were evaluated using a solar simulator (CEP-2000SRR, Bunkoukeiki Inc., AM 1.5G 100 mWcm-2) and a black mask on top of the devices with an exposure area 0.10 cm^2 was used during the photovoltaic measurements. The current-voltage (J-V) curves of these solar cells were measured with a 0.01V/s scanning rate in reverse (from the open-circuit voltage (V_{oc}) to the short-current density (J_{sc})) and forward (from J_{sc} to V_{oc}) modes under standard global AM 1.5 illumination. X-ray Diffraction (XRD) Study. X-ray diffraction analyses (RINT-Ultima III, Rigaku, Japan) were performed in the range 3°−80°. The surface morphology of the samples were observed through a scanning electron microscope (SEM) (JEOL, Neoscope, JCM-6000) and a Bruker Innova atomic force microscopy (AFM) (JSPM-5200). Attenuated Total Reflectance

Fourier transform IR spectras (FT-IR) were tested by FT-IR spectrometer (JASCO, FT/IR-4100 Series) via an attenuated total reflectance (ATR) crystal.

ASSOCIATED CONTENT

Supporting Information.

Additional data and results (SEM images, XRD, photovoltaic parameters of perovskite solar cells) (PDF)

AUTHOR INFORMATION

Corresponding Author

* Email: hayase@life.kyutech.ac.jp.

Present Addresses

† 2-4 Hibikino, Wakamatsu-ku, Kitakyushu 808-0196, Japan

Funding Sources

This work was supported by Core Research for Evolutional Science and Technology (CREST) project of Japan Science and Technology

Notes

There are no conflicts to declare.

REFERENCES

(1) Lee, M. M.; Teuscher, J.; Miyasaka, T.; Murakami, T. N.; Snaith, H. J. Efficient hybrid solar cells based on meso-superstructured organometal halide perovskites. *Science* **2012,** *338* (6107), 643-647.
(2) Leijtens, T.; Eperon, G. E.; Pathak, S.; Abate, A.; Lee, M. M.; Snaith, H. J. Overcoming ultraviolet light instability of sensitized TiO 2 with meso-superstructured organometal tri-halide perovskite solar cells. *Nature communications* **2013,** *4*, 2885.
(3) Liu, M.; Johnston, M. B.; Snaith, H. J. Efficient planar heterojunction perovskite solar cells by vapour deposition. *Nature* **2013,** *501* (7467), 395-398.
(4) Zhou, H.; Chen, Q.; Li, G.; Luo, S.; Song, T.-b.; Duan, H.-S.; Hong, Z.; You, J.; Liu, Y.; Yang, Y. Interface engineering of highly efficient perovskite solar cells. *Science* **2014,** *345* (6196), 542-546.
(5) Domanski, K.; Alharbi, E. A.; Hagfeldt, A.; Grätzel, M.; Tress, W. Systematic investigation of the impact of operation conditions on the degradation behaviour of perovskite solar cells. *Nature Energy* **2018**, 1.
(6) Stranks, S. D.; Eperon, G. E.; Grancini, G.; Menelaou, C.; Alcocer, M. J.; Leijtens, T.; Herz, L. M.; Petrozza, A.; Snaith, H. J. Electron-hole diffusion lengths exceeding 1 micrometer in an organometal trihalide perovskite absorber. *Science* **2013,** *342* (6156), 341-344.
(7) Kojima, A.; Teshima, K.; Shirai, Y.; Miyasaka, T. Organometal halide perovskites as visible-light sensitizers for photovoltaic cells. *Journal of the American Chemical Society* **2009,** *131* (17), 6050-6051.
(8) Yang, W. S.; Park, B.-W.; Jung, E. H.; Jeon, N. J.; Kim, Y. C.; Lee, D. U.; Shin, S. S.; Seo, J.; Kim, E. K.; Noh, J. H. Iodide management in formamidinium-lead-halide–based perovskite layers for efficient solar cells. *Science* **2017,** *356* (6345), 1376-1379.
(9) Xiao, M.; Huang, F.; Huang, W.; Dkhissi, Y.; Zhu, Y.; Etheridge, J.; Gray‐Weale, A.; Bach, U.; Cheng, Y. B.; Spiccia, L. A fast deposition‐crystallization procedure for highly efficient lead iodide perovskite thin‐film solar cells. *Angewandte Chemie* **2014,** *126* (37), 10056-10061.
(10) Park, N.-G.; Grätzel, M.; Miyasaka, T.; Zhu, K.; Emery, K. Towards stable and commercially available perovskite solar cells. *Nature Energy* **2016,** *1*, 16152.
(11) Konstantakou, M.; Perganti, D.; Falaras, P.; Stergiopoulos, T. Anti-solvent crystallization strategies for highly efficient perovskite solar cells. *Crystals* **2017,** *7* (10), 291.
(12) Malinkiewicz, O.; Yella, A.; Lee, Y. H.; Espallargas, G. M.; Graetzel, M.; Nazeeruddin, M. K.; Bolink, H. J. Perovskite solar cells employing organic charge-transport layers. *Nature Photonics* **2014,** *8* (2), 128-132.
(13) Green, M. A.; Ho-Baillie, A.; Snaith, H. J. The emergence of perovskite solar cells. *Nature Photonics* **2014,** *8* (7), 506-514.
(14) Eperon, G. E.; Burlakov, V. M.; Docampo, P.; Goriely, A.; Snaith, H. J. Morphological control for high performance, solution‐processed planar heterojunction perovskite solar cells. *Advanced Functional Materials* **2014,** *24* (1), 151-157.
(15) Chen, Q.; Zhou, H.; Hong, Z.; Luo, S.; Duan, H.-S.; Wang, H.-H.; Liu, Y.; Li, G.; Yang, Y. Planar heterojunction perovskite solar cells via vapor-assisted solution process. *Journal of the American Chemical Society* **2013,** *136* (2), 622-625.

(16) Ahn, N.; Son, D.-Y.; Jang, I.-H.; Kang, S. M.; Choi, M.; Park, N.-G. Highly reproducible perovskite solar cells with average efficiency of 18.3% and best efficiency of 19.7% fabricated via Lewis base adduct of lead (II) iodide. *Journal of the American Chemical Society* **2015,** *137* (27), 8696-8699.
(17) Noh, J. H.; Im, S. H.; Heo, J. H.; Mandal, T. N.; Seok, S. I. Chemical management for colorful, efficient, and stable inorganic–organic hybrid nanostructured solar cells. *Nano letters* **2013,** *13* (4), 1764-1769.
(18) Song, Z.; Abate, A.; Watthage, S. C.; Liyanage, G. K.; Phillips, A. B.; Steiner, U.; Graetzel, M.; Heben, M. J. Perovskite Solar Cell Stability in Humid Air: Partially Reversible Phase Transitions in the PbI2 - CH3NH3I - H2O System. *Advanced Energy Materials* **2016,** *6* (19).
(19) Yang, J.; Siempelkamp, B. D.; Liu, D.; Kelly, T. L. Investigation of CH3NH3PbI3 degradation rates and mechanisms in controlled humidity environments using in situ techniques. *ACS nano* **2015,** *9* (2), 1955-1963.
(20) Tai, Q.; You, P.; Sang, H.; Liu, Z.; Hu, C.; Chan, H. L.; Yan, F. Efficient and stable perovskite solar cells prepared in ambient air irrespective of the humidity. *Nature communications* **2016,** *7*.
(21) Li, G.; Zhang, T.; Zhao, Y. Hydrochloric acid accelerated formation of planar CH 3 NH 3 PbI 3 perovskite with high humidity tolerance. *Journal of Materials Chemistry A* **2015,** *3* (39), 19674-19678.
(22) Troughton, J.; Hooper, K.; Watson, T. M. Humidity resistant fabrication of CH3NH3PbI3 perovskite solar cells and modules. *Nano Energy* **2017,** *39*, 60-68.
(23) Lin, N.; Qiao, J.; Dong, H.; Ma, F.; Wang, L. Morphology-controlled CH 3 NH 3 PbI 3 films by hexane-assisted one-step solution deposition for hybrid perovskite mesoscopic solar cells with high reproductivity. *Journal of Materials Chemistry A* **2015,** *3* (45), 22839-22845.
(24) Atkins, P.; De Paula, J.; Keeler, J. *Atkins' physical chemistry*, Oxford university press: 2018.
(25) Jeon, N. J.; Noh, J. H.; Kim, Y. C.; Yang, W. S.; Ryu, S.; Seok, S. I. Solvent engineering for high-performance inorganic–organic hybrid perovskite solar cells. *Nature materials* **2014,** *13* (9), 897-903.
(26) Yin, M.; Xie, F.; Chen, H.; Yang, X.; Ye, F.; Bi, E.; Wu, Y.; Cai, M.; Han, L. Annealing-free perovskite films by instant crystallization for efficient solar cells. *Journal of Materials Chemistry A* **2016,** *4* (22), 8548-8553.
(27) Bai, Y.; Xiao, S.; Hu, C.; Zhang, T.; Meng, X.; Li, Q.; Yang, Y.; Wong, K. S.; Chen, H.; Yang, S. A pure and stable intermediate phase is key to growing aligned and vertically monolithic perovskite crystals for efficient PIN planar perovskite solar cells with high processibility and stability. *Nano Energy* **2017,** *34*, 58-68.
(28) Burschka, J.; Pellet, N.; Moon, S.-J.; Humphry-Baker, R.; Gao, P.; Nazeeruddin, M. K.; Grätzel, M. Sequential deposition as a route to high-performance perovskite-sensitized solar cells. *Nature* **2013,** *499* (7458), 316-319.
(29) Sun, S.; Salim, T.; Mathews, N.; Duchamp, M.; Boothroyd, C.; Xing, G.; Sum, T. C.; Lam, Y. M. The origin of high efficiency in low-temperature solution-processable bilayer organometal halide hybrid solar cells. *Energy & Environmental Science* **2014,** *7* (1), 399-407.
(30) Im, J.-H.; Lee, C.-R.; Lee, J.-W.; Park, S.-W.; Park, N.-G. 6.5% efficient perovskite quantum-dot-sensitized solar cell. *Nanoscale* **2011,** *3* (10), 4088-4093.
(31) Baikie, T.; Fang, Y.; Kadro, J. M.; Schreyer, M.; Wei, F.; Mhaisalkar, S. G.; Graetzel, M.; White, T. J. Synthesis and crystal chemistry of the hybrid perovskite (CH 3 NH 3) PbI 3 for

solid-state sensitised solar cell applications. *Journal of Materials Chemistry A* **2013,** *1* (18), 5628-5641.
(32) Wang, Y.; Wu, J.; Zhang, P.; Liu, D.; Zhang, T.; Ji, L.; Gu, X.; Chen, Z. D.; Li, S. Stitching triple cation perovskite by a mixed anti-solvent process for high performance perovskite solar cells. *Nano Energy* **2017,** *39*, 616-625.
(33) Salim, T.; Sun, S.; Abe, Y.; Krishna, A.; Grimsdale, A. C.; Lam, Y. M. Perovskite-based solar cells: impact of morphology and device architecture on device performance. *Journal of Materials Chemistry A* **2015,** *3* (17), 8943-8969.
(34) Xiao, Z.; Dong, Q.; Bi, C.; Shao, Y.; Yuan, Y.; Huang, J. Solvent annealing of perovskite‐induced crystal growth for photovoltaic‐device efficiency enhancement. *Advanced Materials* **2014,** *26* (37), 6503-6509.
(35) Ma, Y.; Liu, Y.; Shin, I.; Hwang, I.-W.; Jung, Y. K.; Jeong, J. H.; Park, S. H.; Kim, K. H. Understanding and tailoring grain growth of lead-halide perovskite for solar cell application. *ACS applied materials & interfaces* **2017,** *9* (39), 33925-33933.
(36) Wang, K.; Shi, Y.; Li, B.; Zhao, L.; Wang, W.; Wang, X.; Bai, X.; Wang, S.; Hao, C.; Ma, T. Amorphous Inorganic Electron‐Selective Layers for Efficient Perovskite Solar Cells: Feasible Strategy Towards Room‐Temperature Fabrication. *Advanced Materials* **2016,** *28* (9), 1891-1897.
(37) Ke, W.; Fang, G.; Liu, Q.; Xiong, L.; Qin, P.; Tao, H.; Wang, J.; Lei, H.; Li, B.; Wan, J. Low-temperature solution-processed tin oxide as an alternative electron transporting layer for efficient perovskite solar cells. *Journal of the American Chemical Society* **2015,** *137* (21), 6730-6733.

Graphical Abstract for Table of Contents

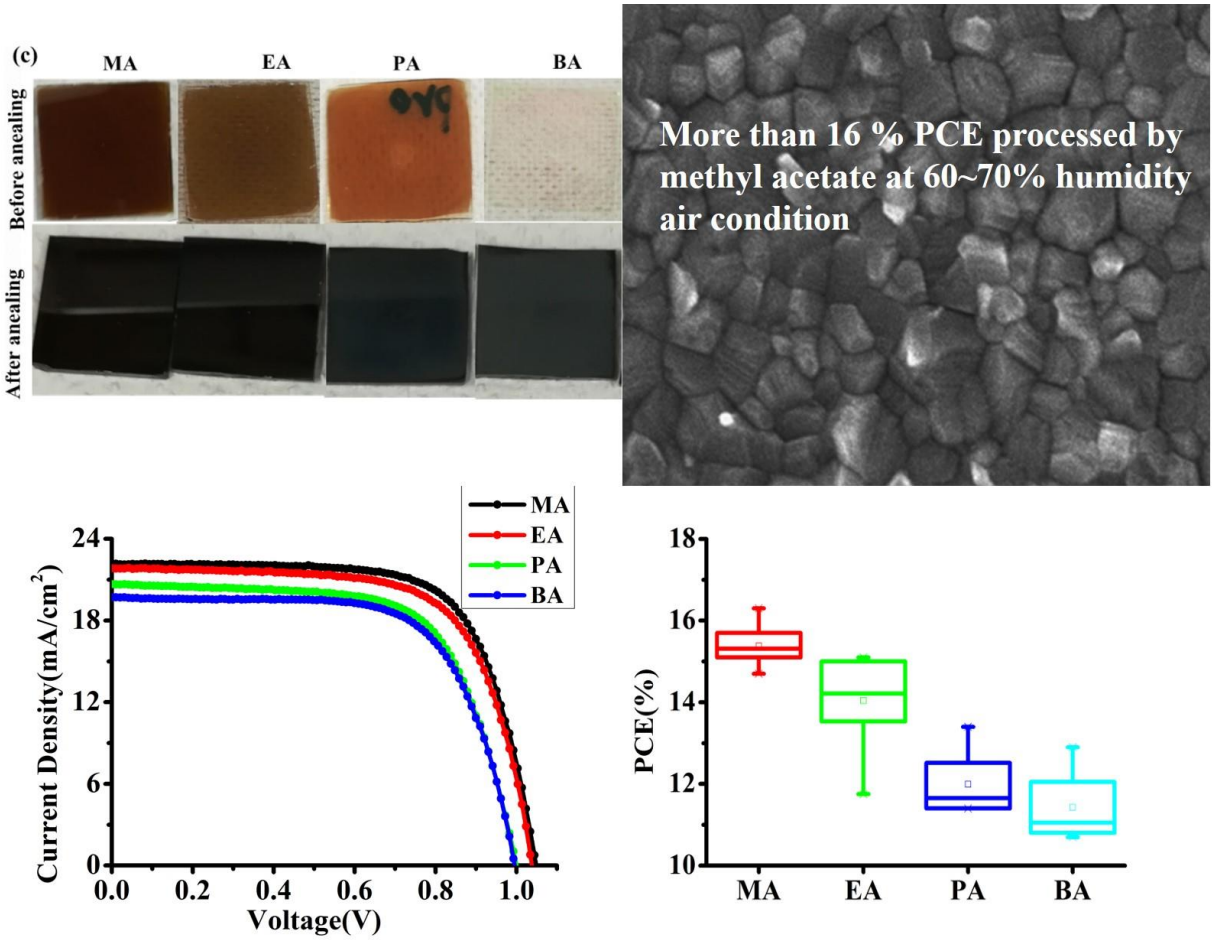

Methyl acetate (MA) leads to the formation of highly dense and pinhole free perovskite films guiding to the best power conversion efficiency of 16.3% with a reduced hysteresis in high humidity air condition.

Supporting Information

Dependence of acetate based anti-solvent for high humidity fabrication of $CH_3NH_3PbI_3$ perovskite devices in ambient atmosphere

Fu Yang, Gaurav Kapil, PuTao Zhang, Zhaosheng Hu, Muhammad Akmal Kamarudin, Tingli Ma, Shuzi Hayase*

Kyushu Institute of Technology, 204 Hibikino Wakamatsu-ku, Kitakyushu 808-0196, Japan

Email: hayase@life.kyutech.ac.jp

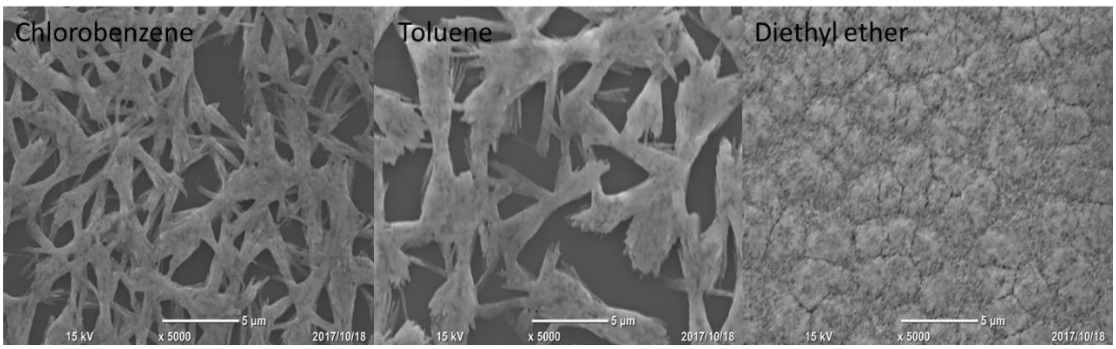

Figure S1 Annealed $CH_3NH_3PbI_3$ film of FTO/Compact SnO2 by different anti-solvents.

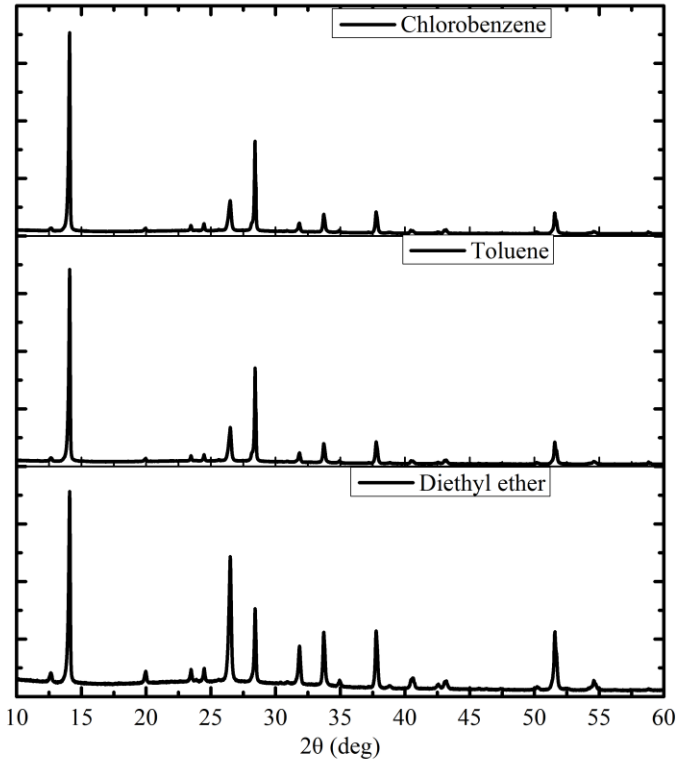

Figure S2 XRD of $CH_3NH_3PbI_3$ film of FTO/Compact SnO_2 by different anti-solvents.

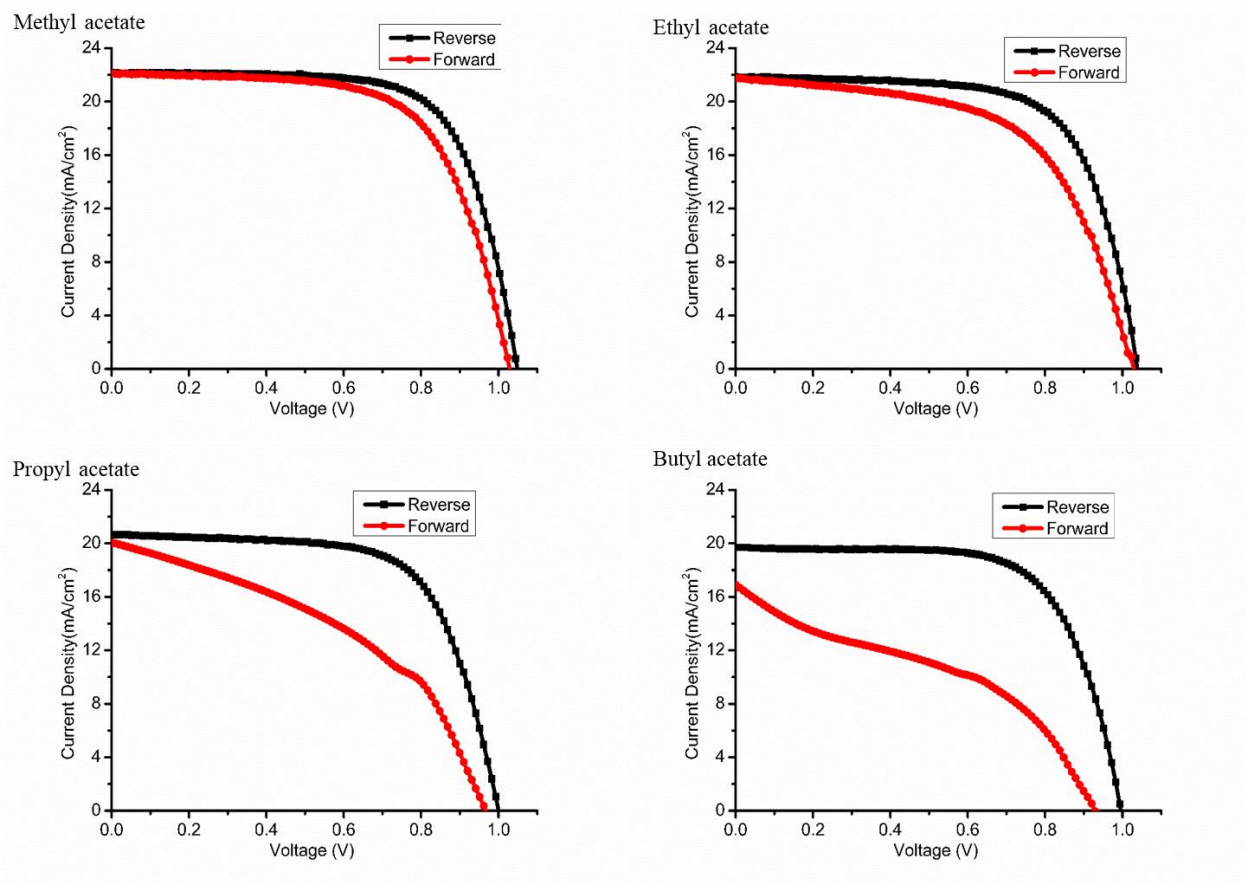

Figure S3 J−V curves of the best-performing perovskite $CH_3NH_3PbI_3$-based solar cell under reverse and forward voltage scans.

Materials	Voc (V)	Jsc (mA cm^{-2})	FF (%)	PCE (%)
Diethyl ether	0.60±0.03	16.02±1.98	53.0±6.5	5.1±1.8
Chlorobenzene	0.45±0.02	0.89±0.22	52.2±7.8	0.2±0.1
Toluene	0.39±0.02	0.81±0.32	57.6±7.2	0.2±0.1

Table S1 Photovoltaic parameters derived from J-V measurements of FTO/c-SnO2/$CH_3NH_3PbI_3$/Spiro-OMeTAD/Au by different anti-solvents.

Materials	Voc (V)	Jsc (mA cm^{-2})	FF (%)	PCE (%)
Methyl acetate	1.03±0.02	20.97±1.02	65.37±4.07	14.8±0.4
Ethyl acetate	0.99±0.03	18.93±1.24	55.25±2.46	9.9±1.7
Propyl acetate	0.84±0.07	14.43±1.26	46.23±4.15	5.1±1.2
Butyl acetate	0.74±0.10	8.81±2.95	38.40±50.34	2.9±1.1

Table S2 Photovoltaic parameters derived from J-V measurements of FTO/c-SnO2/MAPbI3/Spiro-OMeTAD/Au by different contaminated with 2 v% deionized water anti-solvents.

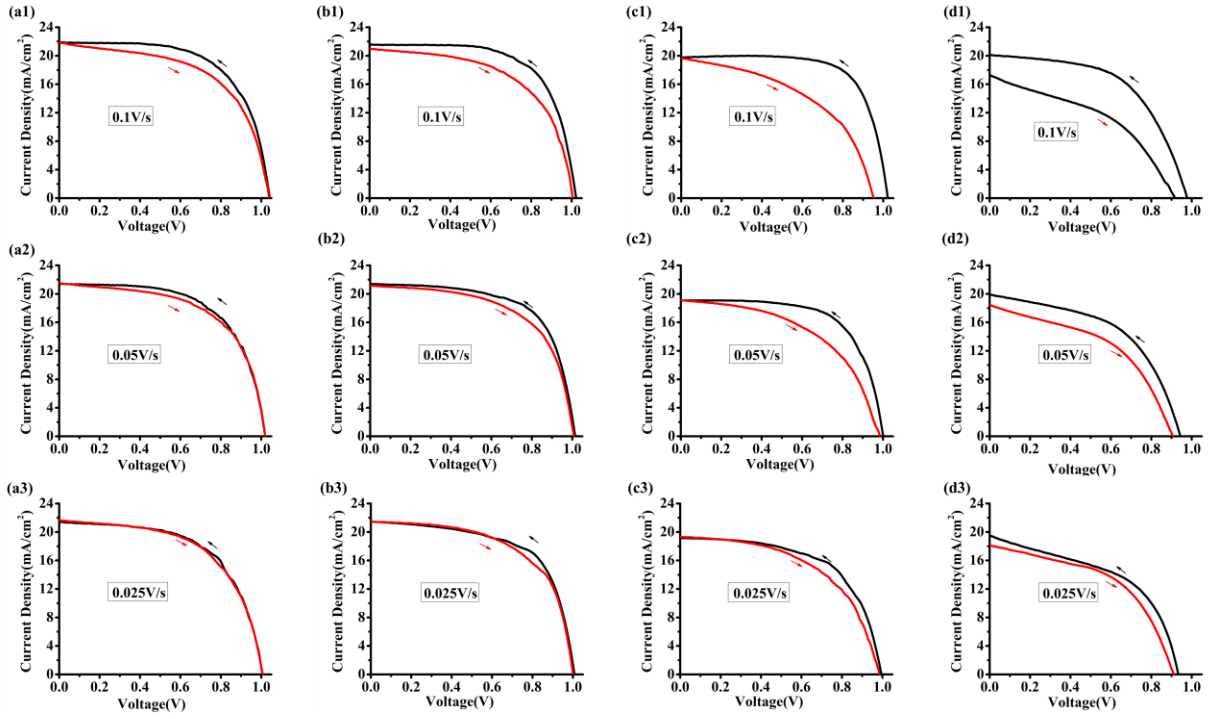

Figure S4 J−V curves of the $CH_3NH_3PbI_3$-based solar cells by different acetate treatment under reverse and forward direction scans by different scan rates of 0.1 V/s, 0.05 V/s and 0.025 V/s. (a1) (a2) (a3), MA; (b1) (b2) (b3), EA; (c1) (c2) (c3), PA; (d1) (d2) (d3), BA.

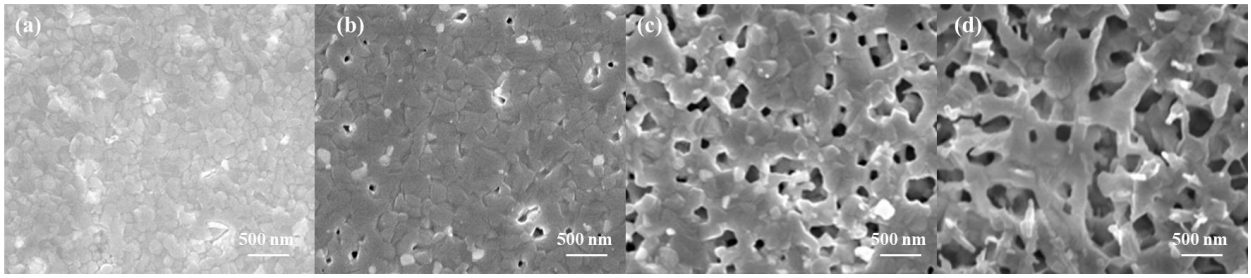

Figure S5 SEM images of annealed CH3NH3PbI3 films of FTO/Compact SnO2 by different anti-solvents with 2v % water. (a) MA; (b) EA; (c) PA; (d) BA.